THEMATIC ISSUE

Emerging hot spot analysis and the spatial–temporal trends of NDVI in the Jing River Basin of China

Bin Xu[1,2,3,4] · Bin Qi[1] · Kai Ji[1] · Zhao Liu[1] · Lin Deng[1] · Ling Jiang[1]

Abstract

As an important indicator of vegetation coverage, the normalized difference vegetation index (NDVI) reflects the changing pattern and evolving trend of the environment. In the Loess Plateau, vegetation plays a critical role in soil and water conservation, which strongly affects the achievement of sustainable development goals. The study of the spatial distribution and temporal trends of NDVI is of great practical importance for the planning of soil and water conservation measures and the evaluation of the environmental situation. In this study, the NDVI, precipitation, land use and land cover data of the Jing River Basin were collected, the emerging hot spot patterns of the NDVI analyzed, the characteristics of spatial distribution and temporal variation of the NDVI in the basin obtained, and the impacts on NDVI from the climate changes and the land cover changes discussed. The results show that the NDVI in Jing River Basin represents a spatial trend of decreasing from northwest to southeast. The emerging hot spot analysis results show that diminishing cold spot, oscillating hot spot and intensifying hot spot are predominant patterns in the basin. The whole basin shows a statistically significant upward trend of high value aggregation of NDVI. The temporal trend of NDVI in the basin varies from − 0.0171 to 0.0185 per year. The increasing trend of vegetation coverage in the basin is statistically significant. The positive correlation between the NDVI and the precipitation mainly observed upstream of the basin reveals that the growth of vegetation in the Loess Plateau is more dependent on the water supply from the precipitation. Land cover transition patterns and the land use patterns also impact the spatial–temporal trends of the vegetation coverage in the basin. The study results may be helpful for the vegetation restoration, soil and water conservation and sustainable development of the Jing River Basin.

Keywords Vegetation cover · Mann–Kendall · Climate change · Anthropological activities

✉ Bin Xu
  xubin@chd.edu.cn

1 School of Water and Environment, Chang'an University, No. 126 Yanta Road, Xi'an 710054, Shaanxi, China

2 Key Laboratory of Degraded and Unused Land Consolidation Engineering, Ministry of Natural Resources, No. 7 Guangtai Road, Xi'an 710075, Shaanxi, China

3 Key Laboratory of Subsurface Hydrology and Ecological Effects in Arid Region, Ministry of Education, Chang'an University, No. 126 Yanta Road, Xi'an 710054, Shaanxi, China

4 Shaanxi Key Laboratory of Land Consolidation, No. 126 Yanta Road, Xi'an 710054, Shaanxi, China

Introduction

Remote sensing is an important technology to quickly obtain the vegetation types and vegetation coverage in a large area, and it can perform long-term dynamic monitoring of vegetation coverage at different scales. Normalized difference vegetation index (NDVI) was proposed by Kriegler et al. (1969) and is one of the most widely used vegetation indices based on remote sensing data, also known as biomass index change, which can separate vegetation from water and soil. It has been widely used in ecological and environmental monitoring, drought monitoring, vegetation growth capacity evaluation, land use, and so on (He et al. 2020; Huang et al. 2021). In recent years, many scholars have conducted more in-depth research on the temporal trend and spatial distribution of vegetation coverage based on the NDVI (Jin et al. 2021).

The Jing River locates in the Yellow River Basin and is the second largest tributary of the Yellow River (Li et al. 2013). The Jing River flows through the Loess Plateau, where soil erosion is serious (Liu et al. 2018). While recharging the Yellow River, it also brings a large amount of sediment to the Yellow River. The Jing River is also the main source of irrigation water for many large irrigation districts in the Guanzhong Plain of Shaanxi Province (Xu et al. 2019; Zhang et al. 2018a). For a long time, the problems of vegetation degradation, soil erosion, runoff reduction, and water pollution in this area have attracted much attention (Li et al. 2014), making it a landmark object for studying soil and water conservation, ecological protection, human health risk assessment, and sustainable development of the Loess Plateau and the Yellow River Basin (Ning et al. 2016; Chang et al. 2016; Li et al. 2018, 2019a, b; He and Wu 2019; Zhang et al. 2020, 2021; Deng et al. 2021). A lot of research work concerning the Jing River Basin has been carried out by scholars worldwide (Li et al. 2013; Liu et al. 2018; Xu et al. 2019).

In the past two decades, through a series of environmental restoration measures such as the Grain for Green Program, the vegetation coverage in the basin has been improved, the spatial distribution of land–water resources has undergone significant changes, and soil erosion has been effectively curbed (Delang and Yuan 2015). However, problems of water shortage, water use conflicts, and ecosystem degradation in the basin still exist. In 2019, ecological protection and high-quality development of the Yellow River Basin have become a national strategic goal in China (Li 2020a, b). Therefore, analyzing the characteristics of vegetation changes in the Jing River under the influence of climate change and anthropological activities is important for optimizing the allocation of regional land–water resources, adjusting soil and water conservation patterns, promoting ecological restoration, and achieving sustainable high-quality development goals in the Yellow River Basin.

The geographical objects and phenomena usually change in both spatial and temporal dimensions. However, in previous studies regarding NDVI variation, the spatial distribution and the temporal trend were analyzed and discussed separately (Li et al. 2013; Liu et al. 2018). The spatial distribution of NDVI mainly reflects the spatial heterogeneity of NDVI in the study area at a specific time, that is, a certain year, a certain month, or a certain day. The temporal trend is mainly obtained through the Mann–Kendall trend test, which usually takes the time series data of points in the study area as the investigating objects. The Mann–Kendall trend test results can only reflect the temporal trend at the points, but cannot analyze the temporal trends at the location between the points. Moreover, the temporal trend can only reveal the overall changing direction and degree throughout the period, and cannot identify the changing patterns of different stages

within the time span. In the view of above issues, it is necessary to introduce new approaches to analyze the change characteristics of NDVI considering the spatial distribution of temporal trends.

Emerging hot spot analysis is a new tool provided by ArcGIS, which can identify spatial–temporal trends and changing patterns of different stages within a time span (ESRI 2021). In recent years, the emerging hot spot analysis has gradually been applied to different scientific fields (Betty et al. 2020; Chambers 2020). However, few studies using the emerging hot spot analysis have been carried out to analyze the NDVI variation and the related factors. This study was conducted for the first time using the emerging hot spot analysis method to analyze the change characteristics of NDVI in the Jing River Basin. This study aims to: (1) analyze the aggregation mode and hot spots trend of vegetation cover in the basin, (2) obtain the spatial–temporal trends of vegetation cover in the study area, and (3) discuss the relationship between vegetation and climate change, and anthropological activities in the basin. This study may provide a meaningful reference for the vegetation restoration, soil and water conservation, and sustainable development of the Jing River Basin.

Materials and methods

Study area

Located in the middle reaches of the Yellow River, the Jing River is a secondary tributary of the Yellow River and the largest tributary of the Wei River (Fig. 1). The Jing River has a total length of 455.1 km and a drainage area of 45,400 km^2 (Li et al. 2013; Liu et al. 2018). It straddles the three provinces (regions) of Gansu, Ningxia, and Shaanxi. The basin is divided into mountainous forest areas in the southwest, mountainous river areas in the southeast, and hilly areas of the Loess Plateau in the central and northern parts (Li et al. 2013; Liu et al. 2018). The basin is a typical temperate continental climate zone, located in the transition zone from a semi-humid climate to a semi-arid climate (Li et al. 2013; Liu et al. 2018). The annual average precipitation from 1981 to 2020 is 508.59 mm, and the annual average temperature is 9.7 °C. The Jing River flows through the high-intensity soil erosion area of the Loess Plateau. A large scope of the basin is covered by thick loess which has poor corrosion resistance. The soil erosion in the basin has been severe for a long time, and the ecological environment is fragile (Li et al. 2013; Liu et al. 2018).

The Jing River Basin exists across the typical agropastoral regions of Northwest China. The dominating land cover is cultivated land, grassland, and forest, with percentages of 47.0%, 32.9%, and 16.5%, respectively. The Jing River Basin

Fig. 1 Location map of the study area

is a very important irrigation water source for large irrigation districts. The proportion of agricultural water consumption exceeds 60% of the total water resources in the basin.
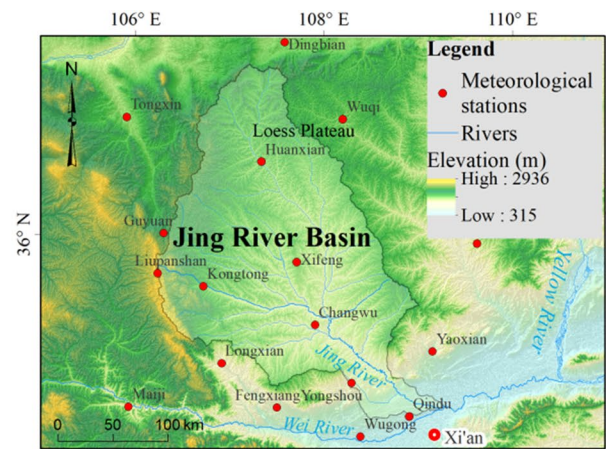
Data

Climate

The daily meteorological data of the Jing River Basin from 1981 to 2020 were collected. Totally, 18 meteorological stations' data were acquired from the China Meteorological Data Service Center (CMDSC 2021). The distribution of the meteorological stations is shown in Fig. 1.

NDVI

The MODIS product was chosen to analyze the spatial and temporal trends of NDVI. The Terra/MODIS Vegetation Indices Monthly L3 Global 1 km SIN Grid datasets were downloaded from the Level-1 and Atmosphere Archive and Distribution System (LAADS 2021) Distributed Active Archive Center (DAAC), located in the Goddard Space Flight Center in Greenbelt, Maryland (https://ladsweb.nascom.nasa.gov/). The data spatial resolution is 1000 m. The annual NDVI of the basin was generated by the maximum value composite (MVC) method.

Land use and land cover

The land use and land cover data were acquired from the website of GlobeLand30 (Jun et al. 2014) (http://www.globallandcover.com/). The GlobeLand30 is a is 30 m spatial resolution global land cover data product, developed by the National Geomatics Center of China (NGCC 2021) and

supervised by the Ministry of Natural Resources of the People's Republic of China.

Digital elevation model (DEM)

The elevation data were obtained from the website of the Consultative Group for International Agricultural Research (CGIAR 2021). The data were measured by the Shuttle Radar Topographic Mission (SRTM) project and produced by NASA. The spatial resolution of the DEM is 3 arc-second (about 90 m).

Methods

Getis-Ord Gi* statistic

Among GIS tools, the Getis-Ord Gi* statistic is widely used for hot spot analysis. By calculating the Gi* statistics of spatial features (spatial variable), it is possible to reflect the aggregation degree of the high-value area (hot spot) and low-value area (cold spot) of the spatial variable (Chambers 2020; ESRI 2021). The calculation is as follows (Getis and Ord 1992; Ord and Getis 1995):

$$G_i^* = \frac{\sum\limits_{j=1}^{n} \omega_{i,j} x_j - \overline{X} \sum\limits_{j=1}^{n} \omega_{i,j}}{S \sqrt{\dfrac{\left[n \sum\limits_{j=1}^{n} \omega_{i,j}^2 - (\sum\limits_{j=1}^{n} \omega_{i,j})^2\right]}{n-1}}}, \tag{1}$$

where x_j is the attribute value for spatial feature j, $\omega_{i,j}$ is the spatial weight between feature i and j, n is the total number of features, and (Getis and Ord 1992; Ord and Getis 1995):

$$\overline{X} = \frac{\sum\limits_{j=1}^{n} x_j}{n}, \tag{2}$$

$$S = \sqrt{\frac{\sum\limits_{j=1}^{n} x_j^2}{n} - (\overline{X})^2}. \tag{3}$$

When the analyzed data is a time series, emerging hot spot analysis can identify the changing trend of the data (Betty et al. 2020; ESRI 2021). For example, it can find new, enhanced, reduced, and scattered hot and cold spots. The emerging hot spot analysis can classify the hot spot as patterns listed in Table 1, which is defined by ArcGIS online help documentation (classifications of the cold spot are similar) (ESRI 2021):

In this study, the Getis-Ord Gi* statistic and the emerging hot spot analysis were implemented by Python and ArcGIS. In the analysis parameter setting, the time-step interval is 1 year, space–time bin size is 1 km, and the neighborhood distance interval is 20 km.

Mann–Kendall trend test

The Mann–Kendall (Mann 1945) trend test method is widely used in many fields of geoscience. It uses the data sequence order to judge the correlation degree between two variables and achieve the variation trend of the long-term data series. The Mann–Kendall trend test statistic can be calculated as follows (Mann 1945):

$$S = \sum_{k=1}^{n-1} \sum_{j=k+1}^{n} \mathrm{sgn}(x_j - x_k), \tag{4}$$

where n is the length of the time series, x_j and x_k are the variable values in the time series ($j > k$). "sgn" is a symbolic function, and (Mann 1945):

$$\mathrm{sgn}(x_j - x_k) = \begin{cases} 1, & x_j - x_k > 0 \\ 0, & x_j - x_k = 0 \\ -1, & x_j - x_k < 0 \end{cases}. \tag{5}$$

The Mann–Kendall trend test uses a significance level of trend (Z), and the slope of the trend (S) to determine the trend significance of data changes. The significance level indicates whether the trend is statistically significant, while the slope shows the degree and direction of the trend. The statistic Z can be calculated as follows (Mann 1945):

$$Z = \begin{cases} \frac{S-1}{\sqrt{\mathrm{VAR}(S)}} & S > 0 \\ 0 & S = 0 \\ \frac{S+1}{\sqrt{\mathrm{VAR}(S)}} & S < 0 \end{cases}. \tag{6}$$

If $Z > 0$, the time series shows a monodic upward trend. If $Z < 0$, the time series shows a monodic downward trend. The absolute critical value of Z for the significance level 0.01, 0.05 and 0.1 are 2.576, 1.96 and 1.645, respectively.

The variance (S) can be calculated by the following equation (Mann 1945):

Table 1 Emerging hotspot patterns and the definitions

Pattern	Definition
No pattern detected	Does not fall into any of the hot or cold spot patterns defined
New hot spot	A location that is a statistically significant hot spot during the final time step and has never been a statistically significant hot spot before
Consecutive hot spot	A location with an uninterrupted run of the statistically significant hot spot bins in the last time step interval. The location has never become a statistically significant hot spot before the final hot spot run and less than 90% of all bins are statistically significant hot spots
Intensifying hot spot	A location that has been a statistically significant hot spot for 90% of the time-step intervals, including the last time step. In addition, the clustering intensity of high counts in each time step increases overall and the increase is statistically significant
Persistent hot spot	A location that has been a statistically significant hot spot for 90% of the time-step intervals with no perceptible trend indicating an increase or decrease in the clustering intensity over time
Diminishing hot spot	A location that has been a statistically significant hot spot for 90% of the time-step intervals, including the last time step. In addition, the clustering intensity in each time step generally decreases and the decrease is statistically significant
Sporadic hot spot	A location that is an on-again then off-again hot spot. Less than 90% of the time-step intervals have been statistically significant hot spots and no time-step intervals have been statistically significant cold spots
Oscillating hot spot	A statistically significant hot spot for the last time-step interval that has a history of also being a statistically significant cold spot during a prior time step. Less than 90% of the time-step intervals have been statistically significant hot spots
Historical hot spot	The most recent time period is not a hot spot, but at least 90% of the time-step intervals have been statistically significant hot spots

$$VAR(S) = \frac{1}{18}[n(n-1)(2n+5)] - \sum_{p=1}^{q} t_p(t_p - 1)(2t_p + 5),$$
(7)

where, q is the number of sets with the same variable value, and t_p refers to data's number in the p_{th} set.

Pearson correlation coefficient

The Pearson correlation coefficient is used to measure the strength of a linear association between two variables, and the equation is as follows (Forthofer et al. 2007):

$$r = \frac{\sum_{i=1}^{n}(x_i - \bar{x})(y_i - \bar{y})}{\sqrt{\sum_{i=1}^{n}(x_i - \bar{x})^2}\sqrt{\sum_{i=1}^{n}(y_i - \bar{y})^2}},$$
(8)

where r represents the Pearson correlation coefficient, x_i denotes the value of the variables x, and y_i is the value of the variable y, $\bar{x}$ refers to the arithmetic mean of variables x, and $\bar{y}$ is the arithmetic mean of variables y. The larger the absolute value of r, the stronger is the correlation. When $r > 0$, it indicates that the two variables are positively correlated, and $r = 1$ means a perfect positive correlation. When $r < 0$, it indicates that the two variables are negatively correlated, and the value $r = -1$ means a perfect negative correlation. When $r = 0$, it indicates that the two variables are not linearly related.

Spatial data interpolation and basic statistical analysis

The daily precipitation data within 1 year were summed up to obtain each station's annual precipitation during the period of 1998–2018. Then, the annual precipitation data were used as the input of the ArcGIS spatial data interpolation tools to generate the spatial distribution raster of the annual precipitation. The main raster interpolation models used in this study are radial basis function and kriging.

Based on the spatial distribution raster of the annual precipitation, the ArcGIS Calculate Statistics tool is used to calculate the min, max, standard deviation, and average of the precipitation of the basin.

Thematic analysis

Figure 2 demonstrates the major logical procedures of the thematic analysis to obtain the emerging hot spot patterns, Mann–Kendall temporal trend, and Pearson correlation coefficient. In ArcGIS, the raster layers of different years' NDVI data are organized as a space–time cube according to the time order. Each cell in the raster layer is located by the column index (col) and row index (row). At the same location (col, row), a single cell of each NDVI layer can be extracted separately, and then the cells of all layers form a data bin. In the data bin, the cells' value that records the annual NDVI can be converted into the NDVI time series data. After that, we use the Getis-Ord method to analyze the time series data and to generate the G_i^* of the location (col, row). Finally, the G_i^* will be recorded as a cell value and saved to the output raster layer of the emerging hot spot patterns. This procedure was directly implemented by the Space Time Pattern Mining Tools in ArcGIS.
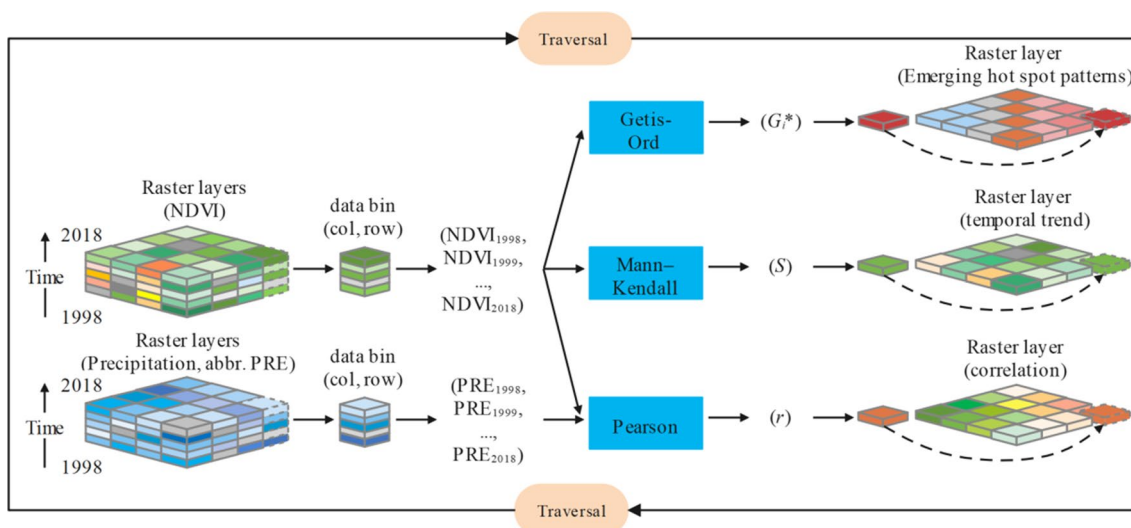

Fig. 2 The logical procedures of the thematic analysis

Using the same logic, set the NDVI time series data as the input of the Mann–Kendall trend test model, and then use Eqs. (4, 5, 6, 7) to calculate the temporal trend and the statistical significance, and save the data to the output raster layer of temporal trend. The procedure is programmed in Python script, and the whole basin is processed by traversal logic.

For the Pearson correlation coefficient, the precipitation data are organized to form a space–time cube like the NDVI data, and then the precipitation time series data of the location (col, row) are extracted. Taking the NDVI time series data and the precipitation time series data as input, Eq. (8) is used to calculate the Pearson correlation coefficient (r) of the location. Finally, r will be recorded as a cell value and saved to the output raster layer of the Pearson correlation coefficient. The procedure is programmed in Python script, and the whole basin is processed by traversal logic.

Results and discussion
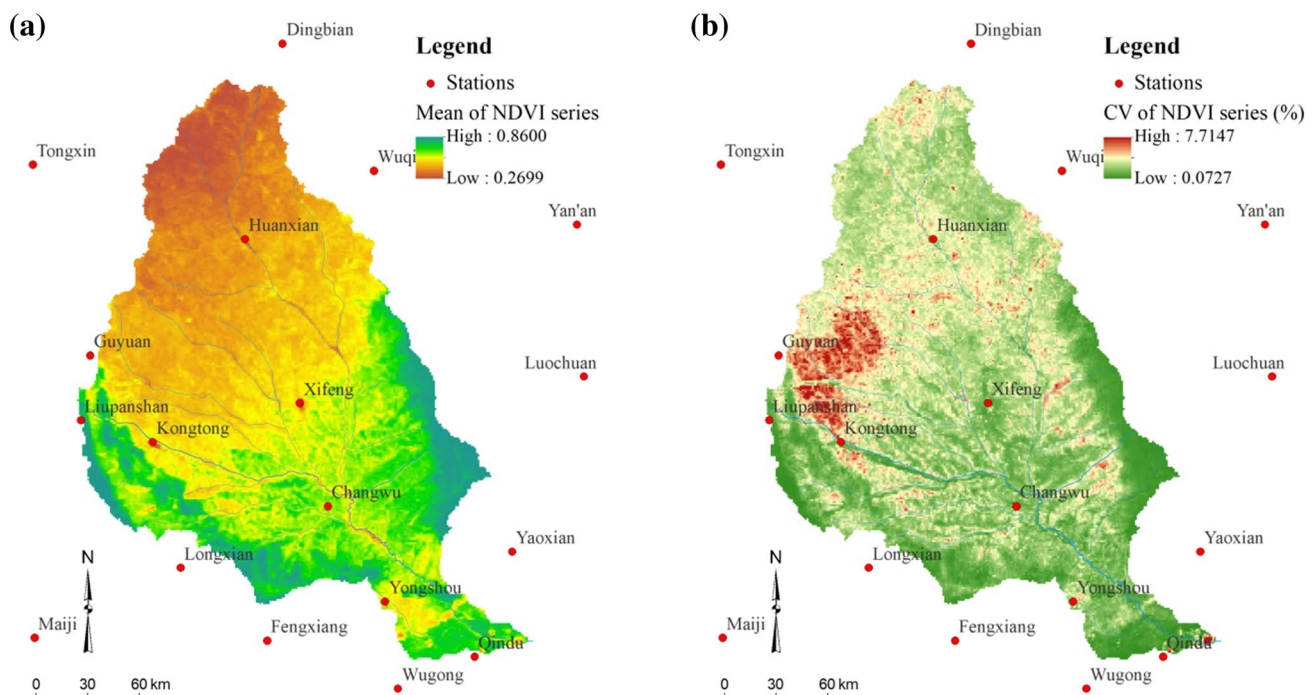
Spatial trend of NDVI

The mean and coefficient of variation (CV) of the NDVI series in the Jing River Basin were generated by calculating the arithmetic mean of each cell in the time series of NDVI raster, and the spatial distribution characteristics of the NDVI statistics in the basin are shown in Fig. 3.

The mean NDVI varies from 0.2699 to 0.8600 with an average of 0.5610, and shows a decreasing trend from southeast to northwest. The two wings of the basin had the highest value of NDVI. The NDVI in the north loess hilly region is the lowest. The zone of NDVI lower than 0.5610 is mainly distributed in the upstream part divided by Guyuan, Kongtong, Xifeng, and Wuqi, which accounts for about 51.67% of the total area of the basin.

The CV of NDVI varies from 0.0727% to 7.7147% (average 1.2776%) and shows an increasing trend from southeast to northwest, which differs from the distribution of mean NDVI. As can be seen in Fig. 3b, there is a local aggregation of the high value of CV at the west of the basin nearby Guyuan and Kongtong, indicating the vegetation coverage there varies more strongly than other places in the basin.

Annual variation characteristics of basin mean NDVI

The annual variation of the NDVI in the Jing River Basin from 1998 to 2018 is shown in Fig. 4. The mean NDVI in the basin is 0.561, the minimum NDVI is 0.128 (2000), and the maximum NDVI is 0.92 (2012). The NDVI anomaly changed from negative to positive in 2010. The annual NDVI shows an upward linear trend with the R^2 coefficient of 0.8363, indicating that the vegetation coverage in Jing River Basin has gradually increased in the past 20 years.

Fig. 3 Spatial distribution of NDVI statistics in the Jing River Basin; **a** mean of NDVI, **b** CV of NDVI
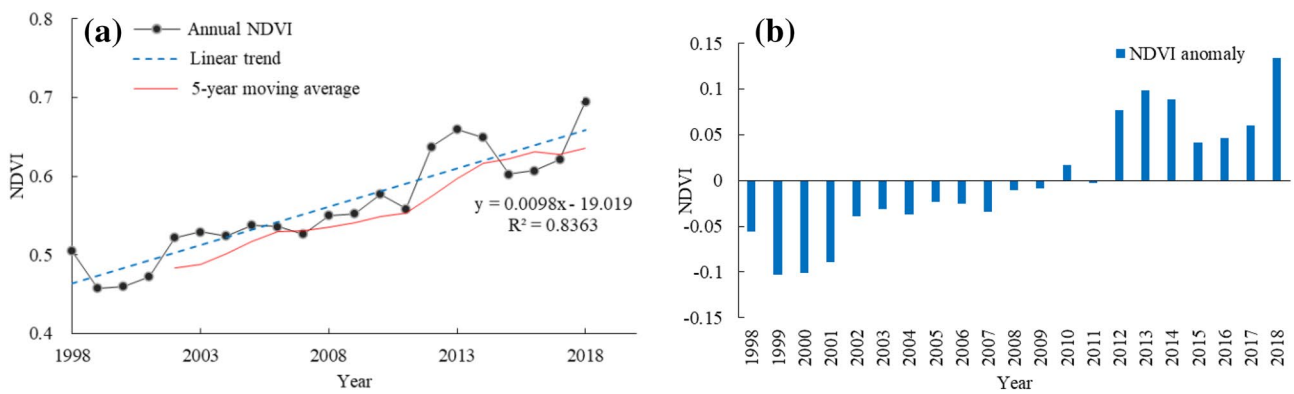
Fig. 4 The change curve of NDVI in the Jing River Basin, **a** annual NDVI and trend, **b** NDVI anomaly
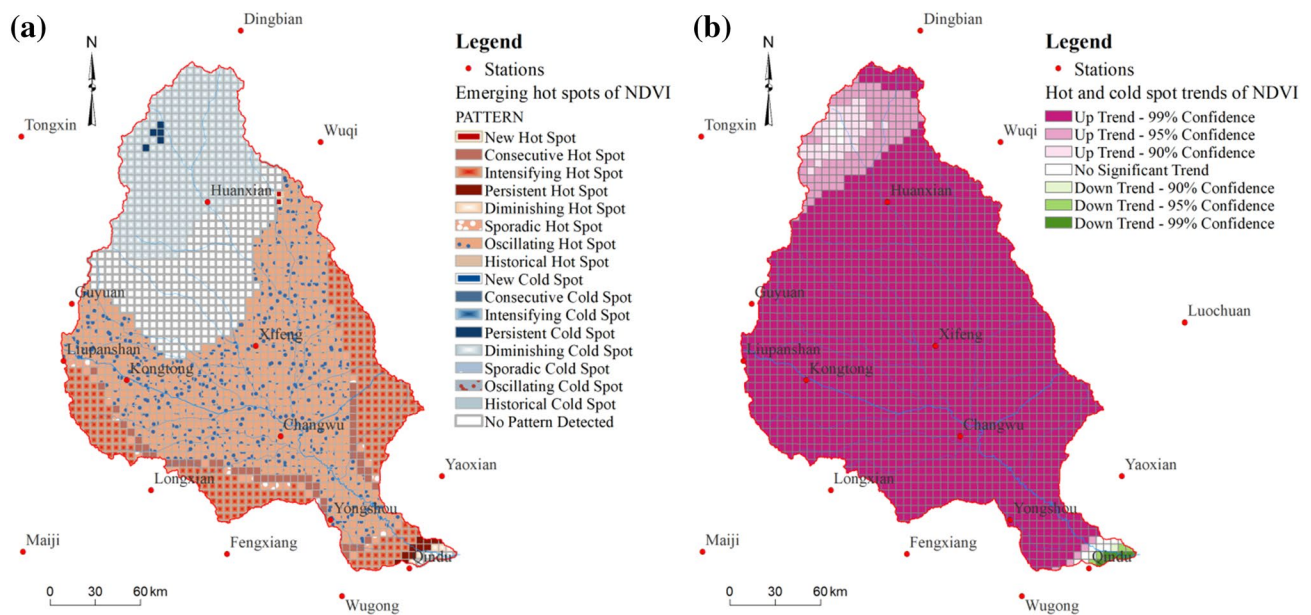

Fig. 5 Emerging hot spot patterns of NDVI in the Jing River Basin, **a** hot spot patterns, **b** hot spot trends

Spatial patterns of NDVI emerging hot spots

Emerging hot spot analysis can reflect the aggregation pattern and trend of vegetation coverage and low NDVI value aggregating as the cold spot of vegetation coverage, while high NDVI value aggregates as the hot spot of vegetation coverage. During a period, the hot spot or cold spot emerges or diminishes with the variation of vegetation coverage. Using the emerging hot spot analysis tool, the time series of NDVI data was analyzed, and the spatial patterns of emerging hot spots of NDVI are depicted in Fig. 5. The NDVI statistics of each hot spot pattern and cold spot pattern are shown in Table 2.

At the upstream of the basin, the primary spatial pattern is diminishing cold spot, indicating that this region has been a statistically significant cold spot of vegetation

Table 2 The NDVI statistics of hot spot pattern and cold spot pattern in the Jing River Basin

Pattern	NDVI			
	MIN	MAX	Mean	STD
New hot spot	0.3539	0.6485	0.5026	0.0800
Consecutive hot spot	0.5262	0.7901	0.6664	0.0777
Intensifying hot spot	0.6507	0.8493	0.7562	0.0580
Persistent hot spot	0.6464	0.7855	0.7155	0.0357
Diminishing hot spot	0.5864	0.7771	0.6910	0.0496
Sporadic hot spot	0.5478	0.7879	0.6748	0.0695
Oscillating hot spot	0.4436	0.7270	0.5887	0.0800
Persistent cold spot	0.2206	0.4766	0.3187	0.0634
Diminishing cold spot	0.2509	0.5525	0.3822	0.0719
No pattern detected	0.3463	0.6556	0.4805	0.0863

coverage for more than 18 years during the whole period, including the year 2018. The intensity of clustering low vegetation coverage in each year is decreasing overall and the decrease is statistically significant. This region accounts for 18.41% of the total area of the basin. In addition, two small persistent cold spots are observed, which have statistically significant low value aggregation of vegetation coverage for 18 years with no discernible trend showing increase or decrease in the clustering intensity of vegetation coverage over time.

In the mid-upstream of the basin, there is a strip between Huanxian and Xifeng that shows no obvious pattern of hot or cold spot, indicating that in this region no obvious aggregation pattern or trends of vegetation coverage were observed in these two decades. This strip accounts for 16.36% of the total area of the basin.

At the central part of the mid-downstream of the basin, from Xifeng to Qindu, large scope of oscillating hot spot is observed, representing the vegetation coverage at this region is high in 2018, but also has a history of low coverage during a prior period, and the period of high vegetation coverage is less than 18 years during the last two decades. This pattern of vegetation coverage trend reaches 44.70% of the total area of the basin.

The intensifying hot spot mainly distributes at the west and east wing of the basin, indicating that the vegetation coverage in these regions keeps high for more than 18 years during the period including 2018 and has a significant increasing trend in each year. The percentage of this pattern in the basin is 14.57%.

In addition, the proportions of the consecutive hot spot, the sporadic hot spot, the persistent hot spot, the diminishing hot spot, and the new hot spot in the basin are 3.00%, 1.87%, 0.47%, 0.27%, 0.22%, and 0.11%, respectively. The new cold spot, the consecutive cold spot, the intensifying cold spot, the sporadic cold spot, the oscillating cold spot, and the historical cold spot are not observed in the basin. The highest mean NDVI is observed in the intensifying hot spot region, while the lowest mean NDVI is observed in the persistent cold spot.

As can be seen from Fig. 5b, almost the entire basin has a statistically significant upward trend in the aggregation of high NDVI values, indicating that vegetation coverage generally increased during this period, whether in hot spots or cold spots.

Temporal trend of NDVI

As presented in the foregoing, the NDVI in the basin has obvious spatial differences and temporal trends. The time series data of the NDVI in the Jing River Basin from 1998 to 2018 are analyzed using the Mann–Kendall test. Figure 6 depicts the spatial distribution of NDVI changing trends and statistical significance.

As shown in Fig. 6a, the variation rate of NDVI in the Jing River Basin is from − 0.0171 to 0.0185 per year, and
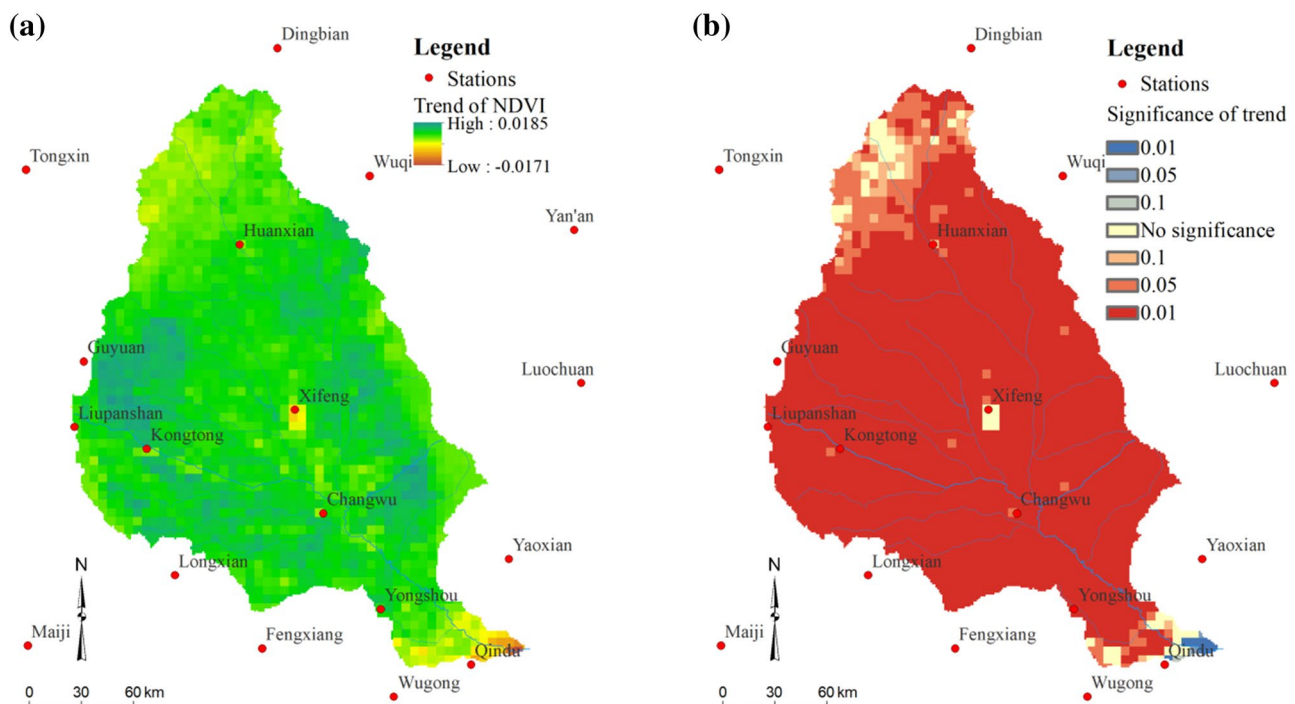
Fig. 6 Spatial distribution of the NDVI temporal trends. **a** Trend of NDVI, **b** significance of trends

the average variation rate is 0.0095 per year. There is no obvious spatial trend of variation rate shown in the basin. However, the distributions of high variation rate are consistent with the distributions of high CV of NDVI. The largest increase is found at Guyuan and Kongtong, and a decreasing trend is found at Qindu.

As can be seen from Fig. 6b, the trend of NDVI shows the significance of $P < 0.05$ and $P < 0.01$ at most of the basin, indicating that the increasing trend of vegetation coverage is significant.

The NDVI temporal trend statistics of each hot spot pattern and cold spot pattern are shown in Table 3. Among all patterns in the basin, only the diminishing hot spot has a negative mean trend of − 0.0046; however, it just accounts for 0.22% of the basin and will not impact the general increasing trend of the vegetation coverage. The government may need to pay more attention to the oscillating hot spot region and the no pattern detected region. The area of these two regions covers more than 60% of the basin. In these two regions, the downward trend is stronger or weaker than

the upward trend alternately, implying that the environment may be unstable and would evolve in an uncertain direction.

Relationships between NDVI and climate and anthropological activities

According to previous similar study results, the NDVI is mainly affected by climate and anthropological activities (Zhang et al. 2018b; Jin et al. 2021).

Climate change

The relationship between the NDVI time series and the precipitation time series was analyzed using the Pearson correlation coefficient. Under the premise of ignoring spatial heterogeneity, Fig. 7 illustrates the general relationship between the regional annual NDVI and the regional annual precipitation of the entire basin. As can be seen in Fig. 7a, the change curves of the NDVI and the precipitation show a similar shape and trend, indicating the potential correlation between the two factors. In Fig. 7b, the upward linear trend with the Pearson correlation coefficient of 0.46 between the NDVI and the precipitation indicates that the NDVI is generally controlled by the precipitation.

The mean and coefficient of variation (CV) of the precipitation series in the Jing River Basin were generated by calculating the arithmetic mean of each cell in the time series of annual precipitation raster, and the spatial distribution characteristics of the precipitation statistics in the basin are shown in Fig. 8.

The mean precipitation varies from 327.2 to 604.5 mm with an average of 512.4 mm and shows a decreasing trend from southeast to northwest. The two wings of the basin had the highest value of precipitation. The precipitation in the north loess hilly region is the lowest.

The CV of precipitation varies from 16.1480 to 25.8485% (average 19.6119) and shows an increasing trend from

Table 3 The NDVI temporal trend statistics of hot spot pattern and cold spot pattern in the Jing River Basin

Pattern	MIN	MAX	Range	Mean	STD
New hot spot	0.0101	0.0117	0.0015	0.0110	0.0007
Consecutive hot spot	0.0007	0.0169	0.0162	0.0111	0.0029
Intensifying hot spot	− 0.0015	0.0185	0.0200	0.0085	0.0032
Persistent hot spot	− 0.0053	0.0054	0.0107	0.0011	0.0028
Diminishing hot spot	− 0.0095	0.0023	0.0118	-0.0046	0.0041
Sporadic hot spot	0.0007	0.0143	0.0137	0.0097	0.0027
Oscillating hot spot	− 0.0024	0.0184	0.0208	0.0108	0.0026
Persistent cold spot	0.0029	0.0053	0.0024	0.0042	0.0006
Diminishing cold spot	0.0017	0.0115	0.0098	0.0066	0.0019
No pattern detected	− 0.0171	0.0171	0.0342	0.0103	0.0031
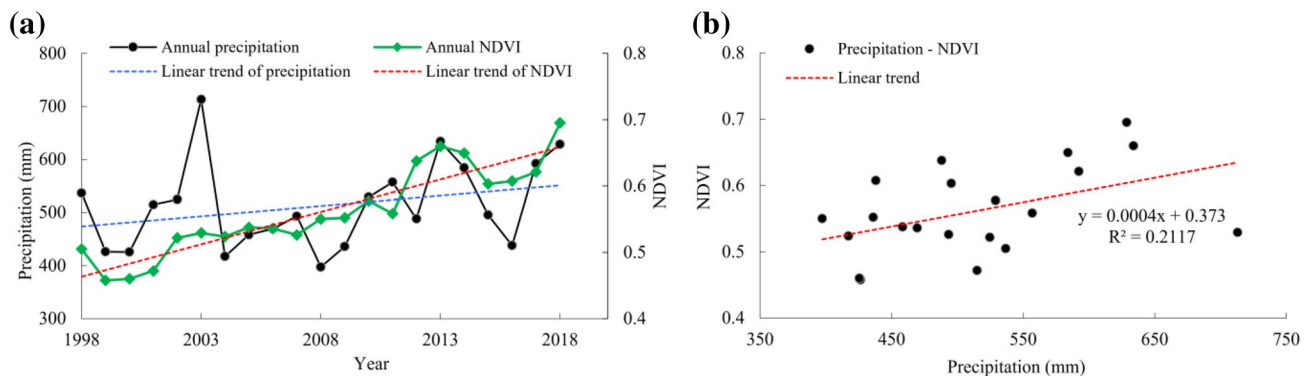
Fig. 7 The relationship between the NDVI and the precipitation in the Jing River Basin, **a** Change curve of the NDVI and the precipitation, **a** annual NDVI and trend **b** Pearson correlation coefficient

(a)

(b)
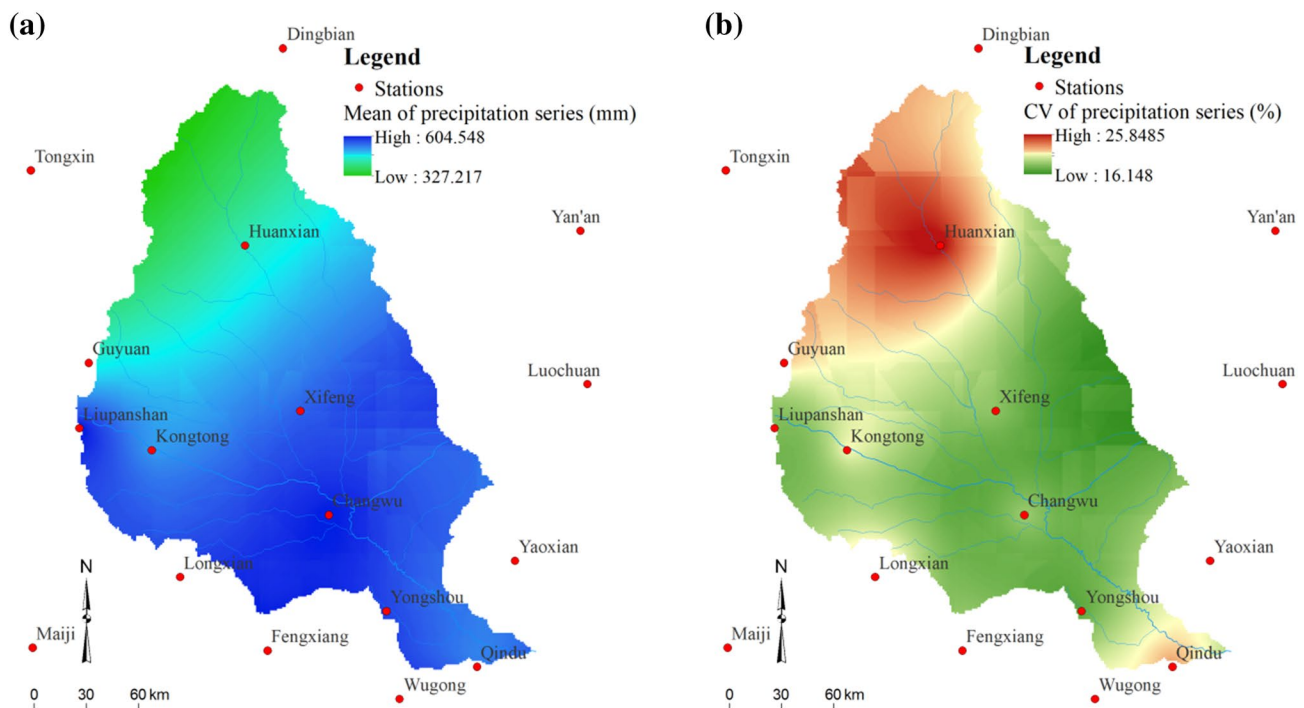
Fig. 8 Spatial distribution of precipitation statistics in the Jing River Basin. **a** Mean of precipitation, **b** CV of precipitation

southeast to northwest. As can be seen in Fig. 8b, a high CV is mainly observed at the north loess hilly region. There is a local aggregation of the high value of CV at Huanxian and the surrounding area, indicating the annual precipitation there varies more strongly than other places in the basin.

The time series data of the precipitation in the Jing River Basin from 1998 to 2018 are analyzed using the Mann–Kendall test. Figure 9 depicts the spatial distribution of precipitation changing trends and statistical significance.

As shown in Fig. 9a, the variation rate of precipitation in the Jing River Basin varies from − 0.2222 to 3.0745 mm per year and the average variation rate is 2.0326 mm per year. A lower variation rate is mainly observed at the two wings of the basin. The largest increasing trend is found at the north loess hilly region.

As can be seen from Fig. 9b, the trend of precipitation shows the significance of $P < 0.1$ and $P < 0.05$ at the north loess hilly region, indicating that the increasing trend of precipitation is significant there.

To study the spatial heterogeneity of the relationship, the spatial distribution of Pearson correlation was generated using the thematic analysis method introduced previously. As shown in Fig. 10, the Pearson correlation coefficient varies from − 0.1121 to 0.8077 with an average of 0.3863. A positive correlation was mainly observed upstream of the basin. In the Loess Plateau, the lower the NDVI, the larger is the correlation between NDVI and precipitation, revealing that the growth of vegetation in this region is more

dependent on the water supply from the precipitation. At the mid and downstream of the basin, the strength of the association is weak, showing that climate change may have limited impacts on the vegetation coverage there during the period. The statistical confidence data signify that the correlation analysis results are statistically significant at the mid and upstream basin, but uncertain at part of the downstream basin.

Figure 11 illustrates the relationship between the NDVI and the precipitation at several typical stations. The upward trends are shown at Huanxian, Liupanshan, and Kongtong, with a medium positive correlation. The downward trends are shown at Xifeng and Changwu; however, the strength of association is very weak.

Anthropological activities

Land use and land cover change are the predominant anthropological activities that will change the vegetation coverage. Using satellite images, major land use and land cover change can be observed on a large scope. As shown in Fig. 12, the land cover change, that is, the increase of the green patches can be found during the period of 2000–2020. In the image of 2010, the land cover area is obviously greater than that of 2000, indicating the increase of vegetation coverage is significant during the period, while the difference in land cover area between 2010 and 2020 is difficult to differentiate.
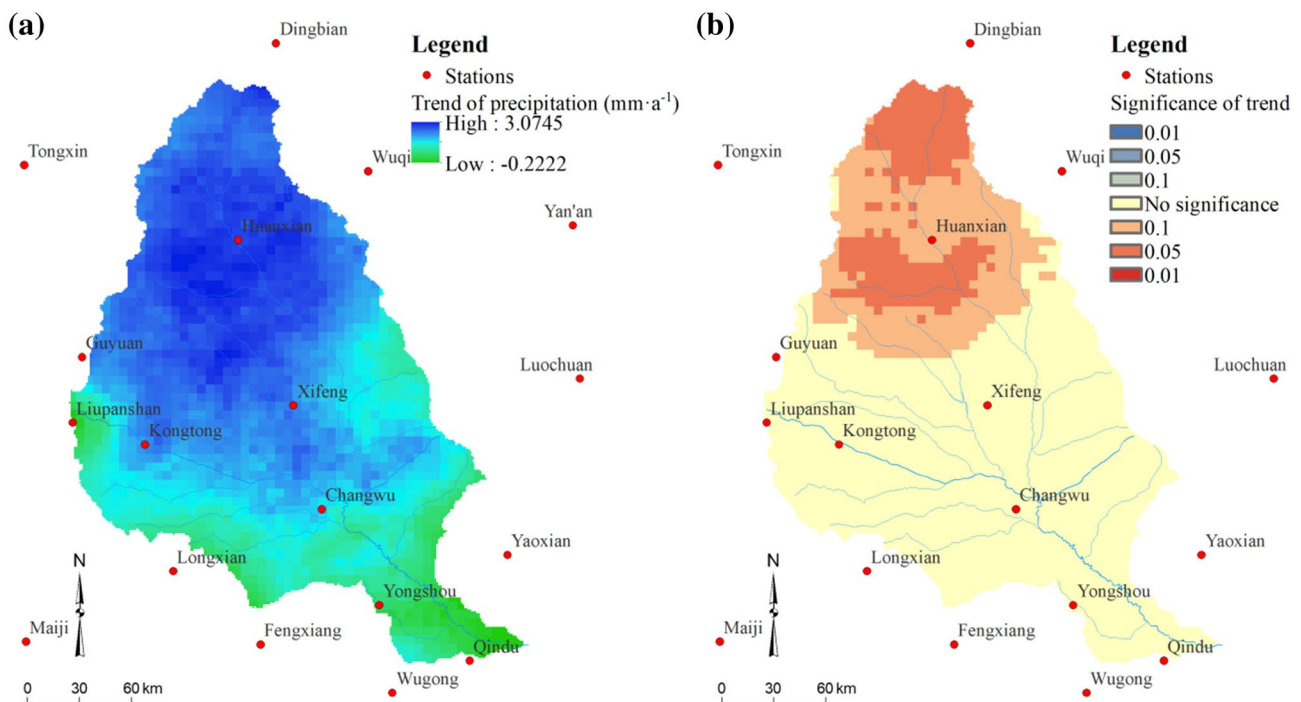
Fig. 9 Spatial distribution of the precipitation temporal trends. **a** Trend of precipitation, **b** significance of trends
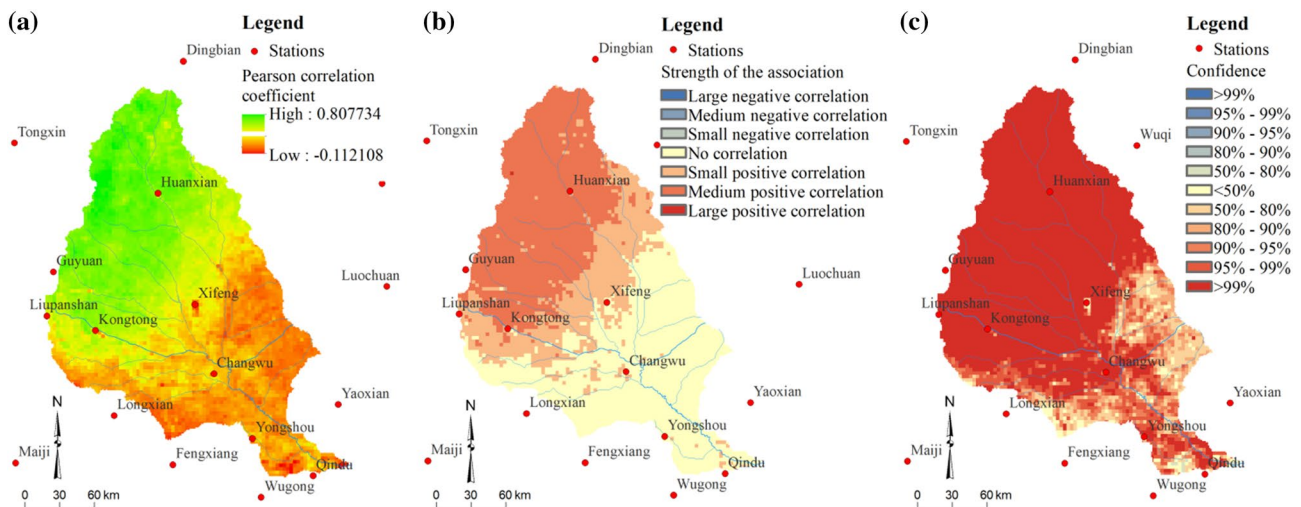

Fig. 10 Spatial distribution of Pearson correlation analysis results in the Jing River Basin, **a** Pearson correlation coefficient, **b** strength of the association, **c** statistical confidence

Therefore, the land use and land cover data of the basin are used to analyze the changing pattern.

Cultivated land, forest, grassland, and shrub are four major land covers that can reflect the regional vegetation coverage. Figure 13 demonstrates the four major land cover transitions that happened in the basin from 2000 to 2020. The statistics of land cover transition are shown in Table 4.

Forest and shrubland mainly transited at the downstream of the basin and cultivated land mainly transited at the upstream of the basin, while grassland mainly transited at the mid and the upstream of the basin. During the period of 2000 to 2020, forest and shrubland increased 0.46% and 0.31%, respectively. Cultivated land and grassland decreased 1.04% and 0.87%, respectively.
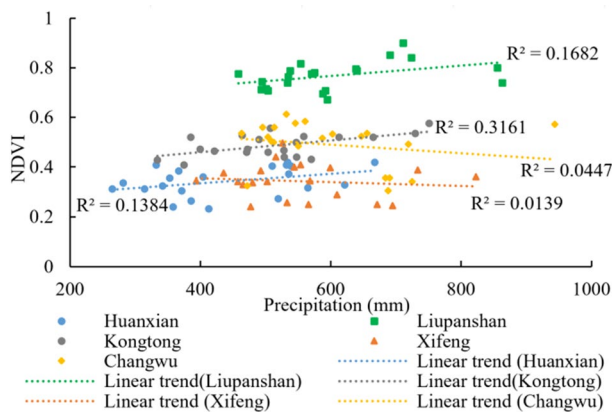
Fig. 11 The relationship between the NDVI and the precipitation at typical stations in the Jing River Basin

As shown in Fig. 14, the primary mixed land cover patterns in diminishing hot spot, no pattern detected region, oscillating hot spot, intensifying hot spot are grassland–cultivated land, cultivated land–grassland, cultivated land–grassland–forest, forest–cultivated land–grassland, respectively. These transition patterns and the primary mixed land cover patterns can explain the spatiotemporal trend of NDVI analyzed previously.

On the views above, the change characteristics and evolving path of NDVI in the Jing River Basin are clear and obvious. According to previous studies, the vegetation change has improved the soil and water conservation situation. Moreover, the increased vegetation, especially the forest, has a positive effect on promoting the capacity of carbon sequestration and oxygen release (Paustian 2014; Wang et al.

2016). However, it has also impacted the runoff of the Jing River and caused water utilization conflict in agricultural development (Zhang et al. 2021). The increased vegetation also consumes more water than before, causing soil moisture loss and the drop in the water table, which affects the growth of some bushs and juvenile trees. Therefore, it is better for the government to strengthen the monitoring of the environment and the ecosystem from a global view, balance the relationship between social development the natural resource management, and ensure the achievement of sustainable development goals.

Conclusions

(1) The spatial distribution characteristics of NDVI indicate that the NDVI in Jing River Basin shows a spatial trend of decreasing from northwest to southeast. The two wings of the basin had the highest value of NDVI. The NDVI in the north loess hilly region is the lowest.

(2) The emerging hot spot analysis results show that diminishing cold spot, oscillating hot spot, and intensifying hot spot are predominant patterns in the basin. The region of no pattern detected also covers a large area of the mid and upstream. The whole basin shows a statistically significant upward trend of high-value aggregation of NDVI, indicating that irrespective of being hot spots or cold spots, the vegetation coverage in these regions has increased overall during the period.

(3) The temporal trend of NDVI in the basin varies from -0.0171 to 0.0185 per year, and the average variation rate is 0.0095 per year. No obvious spatial trend of
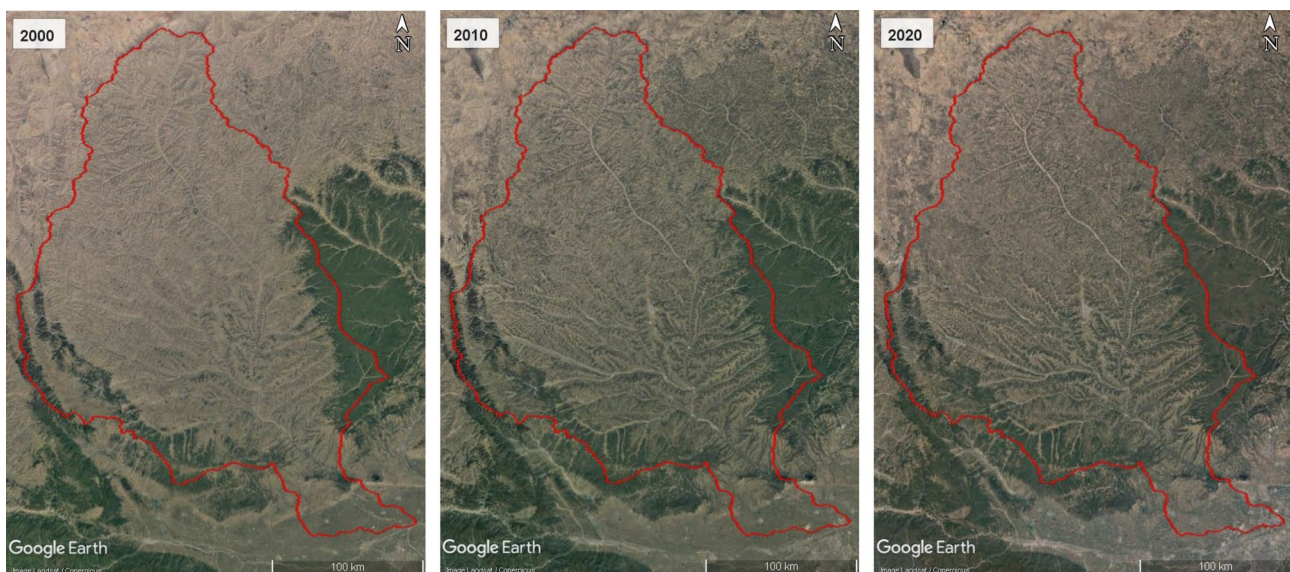
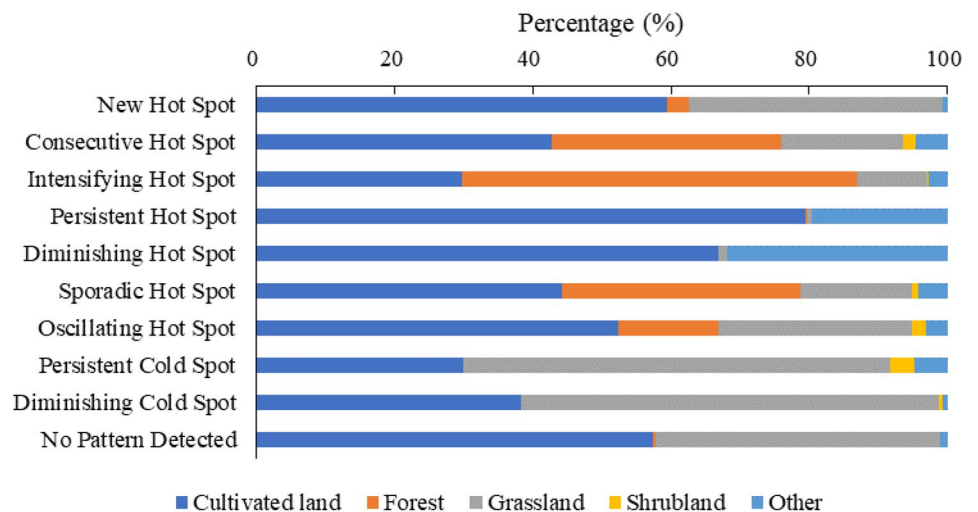**Fig. 12** The satellite images of the Jing River Basin from 2000 to 2020
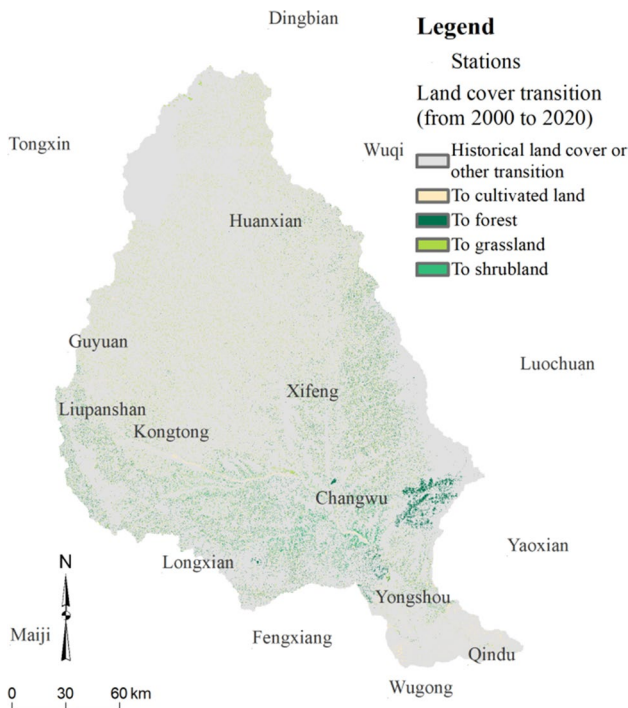
Fig. 13 Land cover transition in the Jing River Basin from 2000 to 2020

variation rate was observed in the basin. The increasing trend of vegetation coverage in the basin is statistically significant.

(4) The positive correlation between the NDVI and the precipitation is mainly observed upstream of the basin. In the Loess Plateau, the lower the NDVI, the larger is the correlation between NDVI and precipitation, revealing that the growth of vegetation in this region is more dependent on the water supply from the precipitation. At the mid and downstream of the basin, the strength of the association is weak, showing that climate change may have limited impacts on the vegetation coverage there during the period.

(5) Anthropological activities have been changing the land cover patterns in the Jing River Basin. During the period of 2000–2020, forest and shrubland have increased 0.46 % and 0.31 %, respectively. Cultivated land and grassland have decreased 1.04 % and 0.87 %, respectively. Land cover transition patterns and the land cover patterns also impact the spatial and temporal trends of the vegetation coverage in the basin.

Table 4 Land cover transition statistics of the Jing River Basin

Category in 2000	Category proportion (%)					Total in 2000
	Cultivated land	Forest	Grassland	Shrubland	Other	
Cultivated land	43.68	0.51	2.29	0.07	1.50	48.05
Forest	0.36	14.23	1.28	0.15	0.02	16.04
Grassland	2.54	1.65	29.12	0.35	0.12	33.77
Shrubland	0.02	0.10	0.15	0.46	0.00	0.73
Other	0.42	0.01	0.06	0.00	0.91	1.40
Total in 2020	47.01	16.50	32.90	1.04	2.55	100.00

Fig. 14 Land cover proportions of hot spot patterns in the Jing River Basin

Data availability Not applicable.

Code availability Not applicable.

Declarations

Conflict of interest The authors declare that they have no known competing financial interests or personal relationships that could have appeared to influence the work reported in this paper.

Ethical approval Not applicable.

Consent to participate Not applicable.

Consent for publication Not applicable.

References

Betty EL, Bollard B, Murphy S et al (2020) Using emerging hot spot analysis of stranding records to inform conservation management of a data-poor cetacean species. Biodivers Conserv 29:643–665. https://doi.org/10.1007/s10531-019-01903-8

CGIAR CG for IAR CGIAR-CSI SRTM—SRTM 90m DEM Digital elevation database. https://srtm.csi.cgiar.org/. Accessed 12 Apr 2021

Chambers SN (2020) The spatiotemporal forming of a state of exception: repurposing hot-spot analysis to map bare-life in Southern Arizona's borderlands. GeoJournal 85:1373–1384. https://doi.org/10.1007/s10708-019-10027-z

Chang J, Li Y, Wei J et al (2016) Dynamic changes of sediment load and water discharge in the Weihe River. China Environ Earth Sci 75:1042. https://doi.org/10.1007/s12665-016-5841-9

China meteorological data service center (2019) Dataset of daily climate data from Chinese surface stations for global exchange (V3.0). http://data.cma.cn/en. Accessed 10 March 2021

Delang CO, Yuan Z (2015) Ecological and environmental impact. In: Delang CO, Yuan Z (eds) China's grain for green program: a review of the largest ecological restoration and rural development program in the world. Springer International Publishing, Cham, pp 135–145

Deng L, Xu B, Yang X, Hu A (2021) Water quality and health risk assessment based on hydrochemical characteristics of tap and large-size bottled water from the main cities and towns in Guanzhong Basin. China Environ Earth Sci 80:139. https://doi.org/10.1007/s12665-021-09415-x

ESRI emerging hot spot analysis—Help|ArcGIS for desktop. https://desktop.arcgis.com/en/arcmap/10.3/tools/space-time-pattern-mining-toolbox/emerginghotspots.htm. Accessed 11 Apr 2021

Forthofer RN, Lee ES, Hernandez M (2007) 13—Linear regression. In: Forthofer RN, Lee ES, Hernandez M (eds) Biostatistics, 2nd edn. Academic Press, San Diego, pp 349–386

Getis A, Ord JK (1992) The analysis of spatial association by use of distance statistics. Geogr Anal 24:189–206. https://doi.org/10.1111/j.1538-4632.1992.tb00261.x

He S, Wu J (2019) Relationships of groundwater quality and associated health risks with land use/land cover patterns: a case study in a loess area, northwest China. Hum Ecol Risk Assess 25(1–2):354–373. https://doi.org/10.1080/10807039.2019.1570463

He S, Li P, Wu J, Elumalai V, Adimalla N (2020) Groundwater quality under land use/land cover changes: a temporal study from 2005 to 2015 in Xi'an, northwest China. Hum Ecol Risk Assess 26(10):2771–2797. https://doi.org/10.1080/10807039.2019.1684186

Huang S, Tang L, Hupy JP et al (2021) A commentary review on the use of normalized difference vegetation index (NDVI) in the era of popular remote sensing. J for Res 32:1–6. https://doi.org/10.1007/s11676-020-01155-1

Jin F, Yang W, Fu J, Li Z (2021) Effects of vegetation and climate on the changes of soil erosion in the Loess Plateau of China. Sci Total Environ 773:145514. https://doi.org/10.1016/j.scitotenv.2021.145514

Jun C, Ban Y, Li S (2014) Open access to Earth land-cover map. Nature 514:434–434. https://doi.org/10.1038/514434c

Kriegler FJ, Malila WA, Nalepka RF, Richardson WD (1969) Preprocessing Transformations and Their Effects on Multispectral Recognition. In Proceedings of the 6th International Symposium on Remote Sensing of Environment, Ann Arbor, MI, USA, 13–16; pp. 97–131

LAADS Level-1 and atmosphere archive and distribution system. https://ladsweb.modaps.eosdis.nasa.gov/. Accessed 12 Apr 2021

Li P (2020a) Meeting the environmental challenges. Hum Ecol Risk Assess 26(9):2303–2315. https://doi.org/10.1080/10807039.2020.1797472

Li P (2020b) To make the water safer. Expo Health 12(3):337–342. https://doi.org/10.1007/s12403-020-00370-9

Li Z, Liu W, Zheng F (2013) The land use changes and its relationship with topographic factors in the Jing river catchment on the Loess Plateau of China. Springerplus 2:S3. https://doi.org/10.1186/2193-1801-2-S1-S3

Li P, Qian H, Wu J, Chen J, Zhang Y, Zhang H (2014) Occurrence and hydrogeochemistry of fluoride in shallow alluvial aquifer of Weihe River. China Environ Earth Sci 71(7):3133–3145. https://doi.org/10.1007/s12665-013-2691-6

Li P, He S, Yang N, Xiang G (2018) Groundwater quality assessment for domestic and agricultural purposes in Yan'an City, northwest China: implications to sustainable groundwater quality management on the Loess Plateau. Environ Earth Sci 77(23):775. https://doi.org/10.1007/s12665-018-7968-3

Li P, He X, Li Y, Xiang G (2019a) Occurrence and health implication of fluoride in groundwater of loess aquifer in the Chinese Loess Plateau: a case study of Tongchuan, northwest China. Expo Health 11(2):95–107. https://doi.org/10.1007/s12403-018-0278-x

Li P, He X, Guo W (2019b) Spatial groundwater quality and potential health risks due to nitrate ingestion through drinking water: a case

study in Yan'an City on the Loess Plateau of northwest China. Hum Ecol Risk Assess 25(1–2):11–31. https://doi.org/10.1080/10807039.2018.1553612

Liu S, Huang S, Xie Y et al (2018) Spatial-temporal changes of rainfall erosivity in the loess plateau, China: changing patterns, causes and implications. CATENA 166:279–289. https://doi.org/10.1016/j.catena.2018.04.015

Mann HB (1945) Nonparametric test against trend. Econometrica 13:245–259. https://doi.org/10.2307/1907187

NGCC NGC of C GlobeLand30. http://www.globallandcover.com/home_en.html. Accessed 12 Apr 2021

Ning T, Li Z, Liu W (2016) Separating the impacts of climate change and land surface alteration on runoff reduction in the Jing River catchment of China. CATENA 147:80–86. https://doi.org/10.1016/j.catena.2016.06.041

Ord JK, Getis A (1995) Local spatial autocorrelation statistics: distributional issues and an application. Geogr Anal 27:286–306. https://doi.org/10.1111/j.1538-4632.1995.tb00912.x

Paustian K (2014) Carbon sequestration in soil and vegetation and greenhouse gases emissions reduction. In: Freedman B (ed) Global environmental change. Springer, Dordrecht, pp 399–406

Wang K, Deng L, Ren Z et al (2016) Dynamics of ecosystem carbon stocks during vegetation restoration on the Loess Plateau of China. J Arid Land 8:207–220. https://doi.org/10.1007/s40333-015-0091-3

Xu B, Zhang Y, Wang J (2019) Hydrogeochemistry and human health risks of groundwater fluoride in Jinhuiqu irrigation district of Wei river basin. China Hum Ecol Risk Assess 25(1–2):230–249. https://doi.org/10.1080/10807039.2018.1530939

Zhang Y, Wu J, Xu B (2018a) Human health risk assessment of groundwater nitrogen pollution in Jinghui canal irrigation area of the loess region, northwest China. Environ Earth Sci 77(7):273. https://doi.org/10.1007/s12665-018-7456-9

Zhang H, Chang J, Zhang L et al (2018b) NDVI dynamic changes and their relationship with meteorological factors and soil moisture. Environ Earth Sci 77:582. https://doi.org/10.1007/s12665-018-7759-x

Zhang Y, Xiong Y, Chao Y et al (2020) Hydrogeochemistry and quality assessment of groundwater in Jinghui canal irrigation district of China. Hum Ecol Risk Assess 26:2349–2366. https://doi.org/10.1080/10807039.2020.1774737

Zhang Y, Chao Y, Fan R et al (2021) Spatial-temporal trends of rainfall erosivity and its implication for sustainable agriculture in the Wei River Basin of China. Agric Water Manag 245:106557. https://doi.org/10.1016/j.agwat.2020.106557